

The Crystal Structure of the Monomeric Human SOD Mutant F50E/G51E/E133Q at Atomic Resolution. The Enzyme Mechanism Revisited

M. Ferraroni¹, W. Rypniewski², K. S. Wilson³, M. S. Viezzoli¹, L. Banci¹
I. Bertini¹ and S. Mangani^{4*}

¹Department of Chemistry
University of Florence, Via
Gino Capponi 9
I-50121 Florence, Italy

²EMBL Outstation, c/o DESY
Notkestraße 85, Hamburg
22603, Germany

³Department of Chemistry
York University, York
YO1 5DD, UK

⁴Department of Chemistry
University of Siena, Pian dei
Mantellini 44, I-53100 Siena
Italy

The crystal structure of the engineered monomeric human Cu,ZnSOD triple mutant F50E/G51E/E133Q (Q133M2SOD) is reported at atomic resolution (1.02 Å). This derivative has about 20% of the wild-type activity. Crystals of Q133M2SOD have been obtained in the presence of CdCl₂. The metal binding site is disordered, with both cadmium and copper ions simultaneously binding to the copper site. The cadmium (II) ions occupy about 45% of the copper sites by binding the four histidine residues which ligate copper in the native enzyme, and two further water molecules to complete octahedral coordination. The copper ion is tri-coordinate, and the fourth histidine (His63) is detached from copper and bridges cadmium and zinc. X-ray absorption spectroscopy performed on the crystals suggests that the copper ion has undergone partial photoreduction upon exposure to the synchrotron light. The structure is also disordered in the disulfide bridge region of loop IV that is located at the subunit/subunit interface in the native SOD dimer. As a consequence, the catalytically relevant Arg143 residue is disordered. The present structure has been compared to other X-ray structures on various isoenzymes and to the solution structure of the same monomeric form. The structural results suggest that the low activity of monomeric SOD is due to the disorder in the conformation of the side-chain of Arg143 as well as of loop IV. It is proposed that the subunit-subunit interactions in the multimeric forms of the enzyme are needed to stabilize the correct geometry of the cavity and the optimal orientation of the charged residues in the active channel. Furthermore, the different coordination of cadmium and copper ions, contemporaneously present in the same site, are taken as models for the oxidized and reduced copper species, respectively. These properties of the structure have allowed us to revisit the enzymatic mechanism.

© 1999 Academic Press

Keywords: enzyme mechanism; mutants; Cu,Zn superoxide dismutase; monomeric superoxide dismutase; X-ray crystal structure

*Corresponding author

Introduction

The structures of proteins as they appear from various investigation protocols under particular experimental conditions represent conformations

Abbreviations used: Cu,ZnSOD, copper,zinc superoxide dismutase; SOD, superoxide dismutase; Q133M2SOD, monomeric human Cu,ZnSOD triple mutant F50E/G51E/E133Q; ESOD, *Escherichia coli* Cu,Zn superoxide dismutase; WT, wild-type.

E-mail address of the corresponding author:
Mangani@unisi.it

corresponding to some of the energy minima among the many available on the conformational energy profile of the system. A collection of structural data on a given protein provides a wealth of information, which allows us to look beyond a single structure and then to propose a model for the structure-function relationship. Such concepts apply particularly well to the enzyme Cu,Zn superoxide dismutase (Cu,ZnSOD) of which a new structural characterization is reported here.

Human Cu,ZnSOD is a homo-dimeric enzyme of 153 residues per subunit that catalyzes the dismu-

tation of two superoxide radicals to molecular oxygen and hydrogen peroxide (Fridovich, 1995; Bertini *et al.*, 1998). The enzymatic reaction occurs through a two-step mechanism involving the reduction and reoxidation of copper(II) (Bannister *et al.*, 1987). The first reported high-resolution X-ray structure on the oxidized dimeric bovine SOD in 1982 was a major breakthrough in the understanding of the relationship between structure and function (Tainer *et al.*, 1982). The eukaryotic Cu,ZnSODs characterized up to now show a completely conserved quaternary structure, being homo-dimeric both in solution and in the solid state. On the contrary, prokaryotic Cu,ZnSODs experience a large variety of structural arrangements, spanning from monomeric forms, as in *Escherichia coli* (Battistoni & Rotilio, 1995), to a dimeric form (but with a different interface with respect to the eukaryotic enzymes; Bourne *et al.*, 1996), to equilibria between monomeric and dimeric forms (Chen *et al.*, 1995). The tertiary structure of one SOD subunit consists of an eight-stranded β -barrel and three long loops containing two very short α -helical segments. The interface between the two subunits is extremely stable due to the large contact area involving both hydrophobic and hydrophilic interactions. The active site is located at the bottom of a channel walled by the external surface of the β -barrel and by two loops. The channel is lined by charged residues providing an electrostatic field gradient which drives the substrate towards the metal site where catalysis occurs. Two metal ions, one Cu(II) and one Zn(II), are bound in the cavity. The crystal structure revealed that the two metals are linked by a histidinato bridge (His63 in the human Cu,ZnSOD consensus sequence which will be used hereinafter) and that the coordination is completed by three more His residues for the copper site and two His residues and one Asp for the zinc site. The ^1H NMR spectra on the cobalt derivative, in which zinc(II) is substituted by cobalt(II), showed that the His arrangement is maintained in solution (Banci *et al.*, 1989b, 1993; Bertini *et al.*, 1993). Several X-ray structures identified a water molecule located at 2.5–3.0 Å from the copper ion (Tainer *et al.*, 1982, 1983; Djinovic *et al.*, 1992; Parge *et al.*, 1992; Rypniewski *et al.*, 1995). Water ^1H NMR data at various magnetic fields have shown that the distance of this water from copper depends on the hydrophobicity of the cavity (Banci *et al.*, 1989a). Molecular dynamics calculations have provided a rationale for this (Banci *et al.*, 1992, 1994).

Chemical evidence (McAdam *et al.*, 1977) and solution ^1H NMR data (McAdam *et al.*, 1977; Bertini *et al.*, 1985, 1991) indicated that the reduced form contains copper(I) bound to only three of the four His residues, with no bridging His. EXAFS data are consistent with this model (Murphy *et al.*, 1997). Conflicting evidence has been reported from crystallographic studies on the reduced bovine enzyme, where the bridge has been found intact despite the fact that bond length values and EPR

data on the crystals indicate that the copper is indeed copper(I) (Rypniewski *et al.*, 1995). An X-ray report on an initially oxidized form revealed a broken bridge with a copper-His63 $\text{N}^{\epsilon 2}$ distance of 3.1 Å (average of three structures; Ogihara *et al.*, 1996). This distance is shorter than the contact distance, but it does not correspond to a coordination bond. It was concluded that the structure represented a reduced species, the reduction taking place upon crystallization (Ogihara *et al.*, 1996). Two more crystal structure determinations, one on a mutant enzyme found in FALS patients (Hart *et al.*, 1998) and one on a dithionite reduced bovine enzyme at pH 5.0 (Ferraroni *et al.*, 1998), revealed a difference in copper environment between the two SOD subunits: one subunit has the copper tetra-coordinated and the bridge intact, and the other the copper tri-coordinated and the bridge broken. Also the recently determined crystal structure of the natural monomeric Cu,ZnSOD from *E. coli* (ESOD) shows a long Cu-His63 $\text{N}^{\epsilon 2}$ distance (2.65 Å) occurring in the oxidized form of the enzyme (Pesce *et al.*, 1997). This has been later interpreted as due to photoreduction of copper (Stroppolo *et al.*, 1998). Finally, the solution structure of an engineered monomeric triple mutant of human Cu(I),ZnSOD has been determined by ^1H NMR (Banci *et al.*, 1998). The Cu,ZnSOD monomer has been produced by replacing both Phe50 and Gly51 residues at the subunit interface with Glu (Bertini *et al.*, 1994). The active site channel residue Glu133 was further modified with Gln. This mutant, called Q133M2SOD hereinafter, has an activity which is 20% that of the wild-type (WT) enzyme (Banci *et al.*, 1997). The mutant solution structure again provided evidence of protonated His63 and a model for the copper(I) coordination sphere with a Cu(I)-His63 $\text{N}^{\epsilon 2}$ average distance of 3.5 Å.

Taken together, the above studies raised a number of new fundamental questions concerning the structural differences of the copper site between oxidized and reduced Cu,ZnSOD forms and how they can be fitted into a satisfactory structure-based framework for the enzymatic mechanism. In addition, a more general question regards the role of the protein matrix in dictating the metal coordination. The results of the present crystal structure determination of the monomeric Q133M2SOD mutant are highly relevant in this context. The protein was crystallized in the presence of high concentration of CdCl_2 . We find a cadmium-substituted species where cadmium substitutes copper in a coordination environment typical of the oxidized protein, and at the same time an unsubstituted species in which copper is coordinated as observed in the solution structure of the reduced analogue. We report here this structure determined at atomic resolution (1.02 Å), discuss the results in terms of a model going beyond a single structure, and revisit the proposed enzymatic mechanisms. Finally, we try to address the question as to why cytoplasmic SOD is a

multimeric enzyme, and the effect of monomerization on the structure of the active site cavity.

Results

Accuracy of the model

The crystal structure of Q133M2SOD has been determined to 1.02 Å resolution by using synchrotron radiation, solved by molecular replacement and refined by full-matrix least-squares procedures to a final *R*-factor of 0.118. The rms coordinate error obtained from least-squares is 0.039 Å for main-chain atoms, while the overall rms coordinate error for all the atoms, including water molecules, is 0.065 Å. The largest errors occur in the least defined regions of the structure located in loop IV (disulfide bridge region, where the highest values in the range 0.100–0.200 Å are for residues 57–63). The final rms values of the electron density in the $3F_o - 2F_c$ and $F_o - F_c$ maps, calculated with $F_{000}/V = 0.23 \text{ e}^- \cdot \text{Å}^{-3}$, are 0.56 and 0.08 $\text{e}^- \cdot \text{Å}^{-3}$ respectively. The electron density in the $F_o - F_c$ map showed the positions of many of the hydrogen atoms before their contribution was introduced in the structure factor calculation. The Ramachandran plot (Ramachandran & Sasisekharan, 1968) for the structure shows that 88.5% of non-glycine or proline residues lie in the most favored regions of the plot, while 11.5%, fall within the allowed regions as defined in the program PROCHECK (Laskowski *et al.*, 1993).

Description of the final model

Figure 1 shows a sketch of the present structure where the secondary structure elements are labeled as described by Getzoff *et al.* (1989), and the residues involved in subunit-subunit interactions in the WT dimeric enzyme are highlighted. The final model contains 1166 non-hydrogen protein atoms, 1145 hydrogen atoms, 284 water molecules, the active site copper, cadmium and zinc ions, and a further eight cadmium and two chloride ions. The overall folding and structure of the protein closely matches that of a subunit of the dimeric WT protein (1SOS; Parge *et al.*, 1992; Figure 2), except for loop IV which is disordered and where the short α -helix, observed in the WT enzyme between residues Ala55–Gly61, is lost. The characteristic Greek-key β -barrel motif of the folding is maintained as shown in Figure 1. Least-squares superposition of the C^α atoms of the two structures gave an rms deviation of 0.96 Å and a maximum deviation of 4.71 Å for Asn53. The only significant differences occur for the residues 51–60, 108–110, 130–131, and the N and C termini which, in the wild-type dimeric protein, are mainly involved in the subunit-subunit interface.

In the β -sheet regions of the molecule the electron density is well defined and the maps clearly show the individual atoms. An example is shown in Figure 3 where the electron density map for

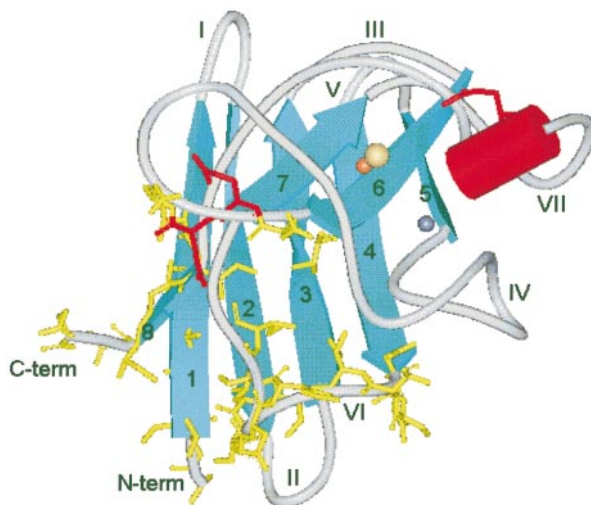


Figure 1. Schematic view of the Q133M2SOD structure displaying the secondary structure elements numbered by Getzoff *et al.* (1989). The side-chains of the residues homologous to those involved in the subunit-subunit interface in the WT dimer are shown as yellow sticks. The mutated residues E50, E51, Q133 are shown as red sticks. Orange, yellow and gray spheres of arbitrary radius represent copper, cadmium and zinc ions, respectively.

Phe20 is reported. Conversely, many loop regions are poorly defined, the electron density being less than $0.28 \text{ e}^- \cdot \text{Å}^{-3}$ in the $3F_o - 2F_c$ map, and the refined temperature factors are high for at least one of the side-chain atoms. The disulfide bridge region of loop IV (residues 53–61) is poorly defined also for the main-chain atoms. The atoms for these residues were introduced in the model just in the last stage of the anisotropic refinement, when the better agreement between F_o and F_c provided interpretable electron density. The side-chains of 13 residues and the carbonyl oxygen atom of Gly33 have two conformations which have been successfully modeled. The disorder for Cys57 reveals interesting aspects. One of the modeled conformations of this residue is such that its backbone carbonyl oxygen atom is no longer involved in a hydrogen bond with the N^ϵ of Arg143, which is conserved in all previously determined structures, and keeps the side-chain of the latter amino acid properly oriented in the enzyme active site cavity. This is likely to be the origin of the observed Arg143 side-chain disorder (see below). There is no electron density for the side-chain atoms of residues Glu77, Glu78, Lys91, Lys122 that were excluded from the model. Most of the disordered residues or residues with a double conformation are either lysine residues or lie at the enzyme surface and are involved in intermolecular contacts. From the comparison with the dimeric form it appears that the mutations performed to obtain the monomer have not perturbed the overall tertiary structure of the protein, although the loop IV, where two of them reside, is a heavily disordered

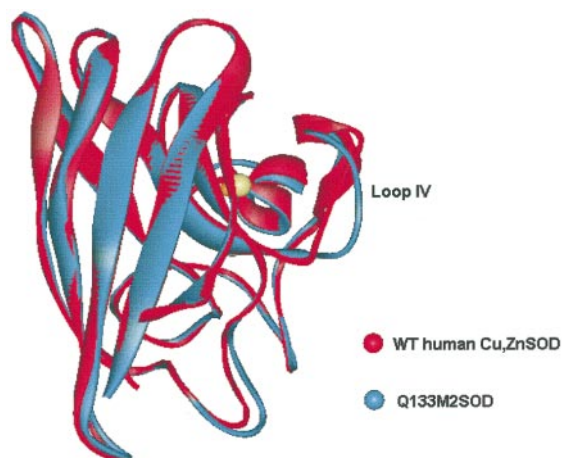


Figure 2. Comparison, by least-squares superposition of C^{α} atoms, between Q133M2SOD (blue) and a subunit of 1SOS (WT HSOD, red; Parge *et al.*, 1992). The differences in loop IV conformations are evident.

part of the enzyme. It may be worth noting that the packing of Q133M2SOD molecules in the crystal reproduces neither the eukaryotic nor the prokaryotic dimers.

The average temperature factor of the final model is 14.8 \AA^2 for main-chain atoms and 20.1 \AA^2 for side-chain atoms. The cadmium ions, which were used in the crystallization medium in order to obtain highly ordered crystals are coordinated, besides to the active site, to side-chain atoms of the enzyme surface residues, usually glutamate or aspartate and just in one case to the imidazole ring of His110. Their coordination spheres are completed with water molecules or chloride anions. The coordination number is usually six with octahedral geometry. The binding sites for cadmium atoms lie on the mutant surface in those regions that are involved in intermolecular interactions. The cadmium ions mediate contacts between molecules in the crystal and this can be the reason for their efficiency in promoting formation of well-ordered crystals diffracting at high resolution. The occupancy factors for each cadmium ion were refined resulting in fractional occupancies between 0.23 and 0.83, the occupancies increasing with the number of protein ligand atoms.

The metal sites

The side-chain atoms of the residues coordinated to the metal ions are well ordered. The electron density for each atom of these residues in the $3F_o - 2F_c$ map is above $1.12 \text{ e}^- \cdot \text{\AA}^{-3}$ level as shown in Figure 4(a) and (b). Figure 5 shows the metal coordination environment. The coordination bond distances and angles concerning the metals in the active site cavity are reported in Table 1 in comparison with the values determined for one subunit of the WT dimeric enzyme and for ESOD. While the coordination around the Zn(II) ion is similar to

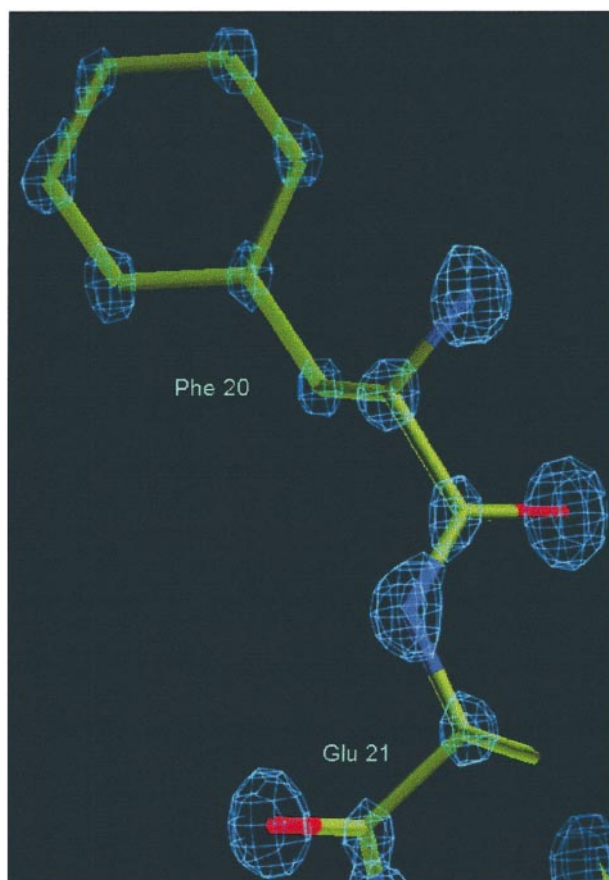


Figure 3. Electron density map of the Phe20 residue, computed with $3F_o - 2F_c$ coefficients and phases from the refined model contoured at 3σ ($1.68 \text{ e}^- \cdot \text{\AA}^{-3}$), showing the model at atomic resolution.

that in the native human enzyme, two different electron density peaks, at a level higher than $1.0 \text{ e}^- \cdot \text{\AA}^{-3}$ in the initial $F_o - F_c$ map and about 1.6 \AA apart from each other, are present in the copper site. These peaks are clearly seen in the $3F_o - 2F_c$ map shown in Figure 4, and are due to two metal ions sharing the site with fractional occupancy. They can be interpreted considering that a cadmium ion, from the crystallization solution, partially replaces copper in the catalytic site. The atom types of the two electron density peaks were assigned on the basis of the coordination number, geometry and bond lengths (Table 1). For one site the coordination number is six and the geometry is octahedral, with bond distances longer than those expected for a copper(II) ion and typical of cadmium(II) coordination compounds (Orpen *et al.*, 1989). The other peak is assigned to a copper(I) ion on the basis of the metal coordination. The occupancy factors for these two metal ions were refined and converged to a value of 0.41 and 0.45 \AA^2 for copper and cadmium, respectively. Unexpectedly, the copper ion is bound to only three histidine ligands, i.e. His46, His48, and His120. His63, which bridges the two metal ions in

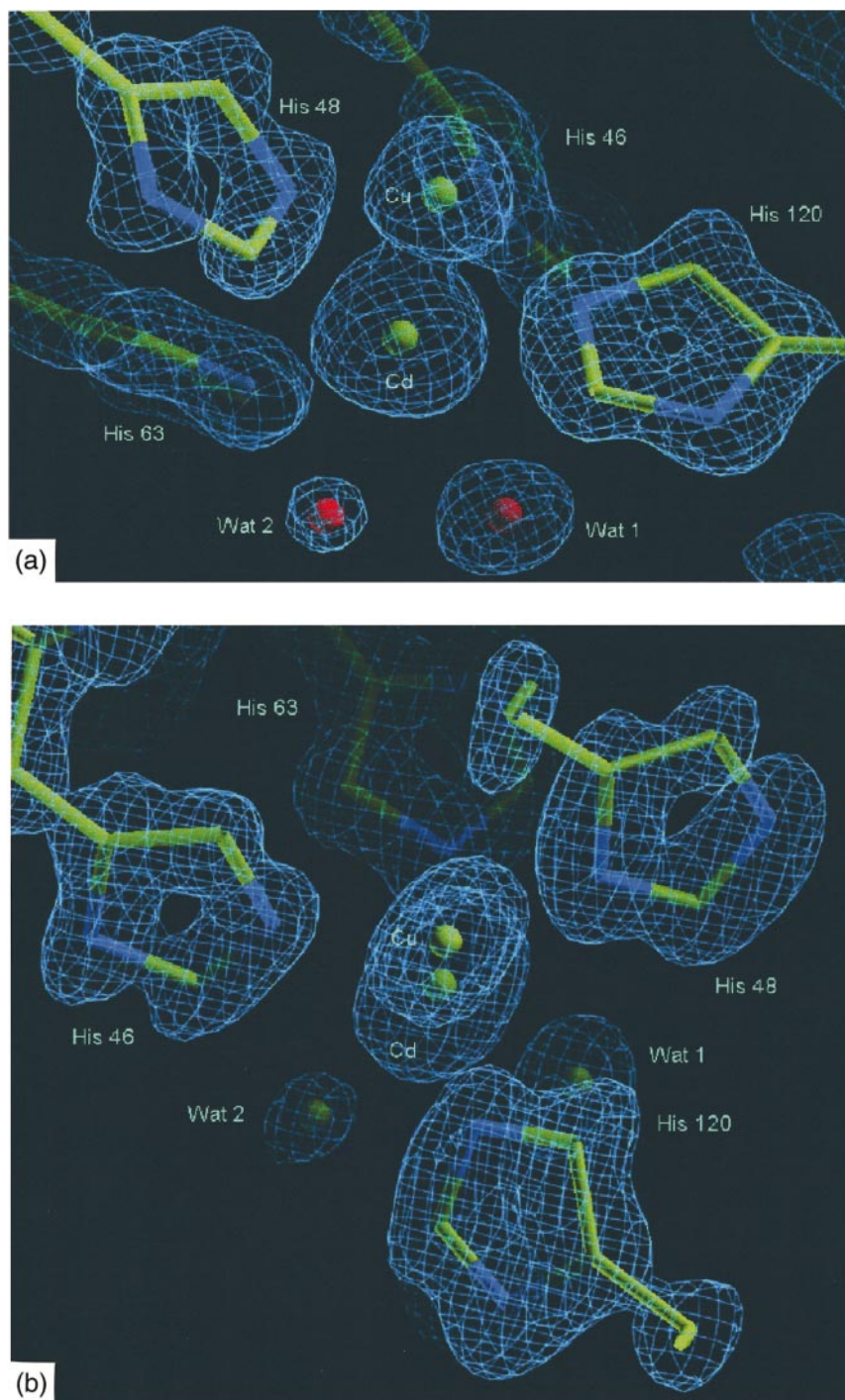


Figure 4. The (a) cadmium and (b) copper sites shown by a $3F_o - 2F_c$ electron density map from the atomic resolution data set, contoured at 2σ ($1.28 \text{ e}^- \cdot \text{\AA}^{-3}$) superimposed to the final model.

the human oxidized dimeric WT SOD as well as in the present cadmium derivative, is rotated away from copper, with a Cu-N^{e2} distance of 3.31 Å. The rmsd of the side-chain atoms of His63 is 0.6 Å and 0.3 Å for the main-chain atoms, with respect to the human oxidized dimeric WT SOD, indicating that the position of this residue has remained essentially unchanged with respect to the dimeric oxidized SOD with only a small rotation of the imidazole ring around the C^β-C^γ bond, resulting in a 0.8 Å difference of the His63 N^{e2} position

between the mutant and dimeric WT SOD enzymes. The copper ion is displaced by about 1 Å with respect to its position in the human oxidized dimeric WT enzyme in a direction opposite to that of His63 N^{e2}. The effect of these two concomitant movements is a lengthening of the Cu-N^{e2} distance. The Cu-(His)₃ cluster is essentially planar with the copper atom deviating from the plane of the three histidine nitrogen atoms by only 0.10 Å. The positions of the His46 and His48 imidazole ring centres are displaced from those in the WT SOD

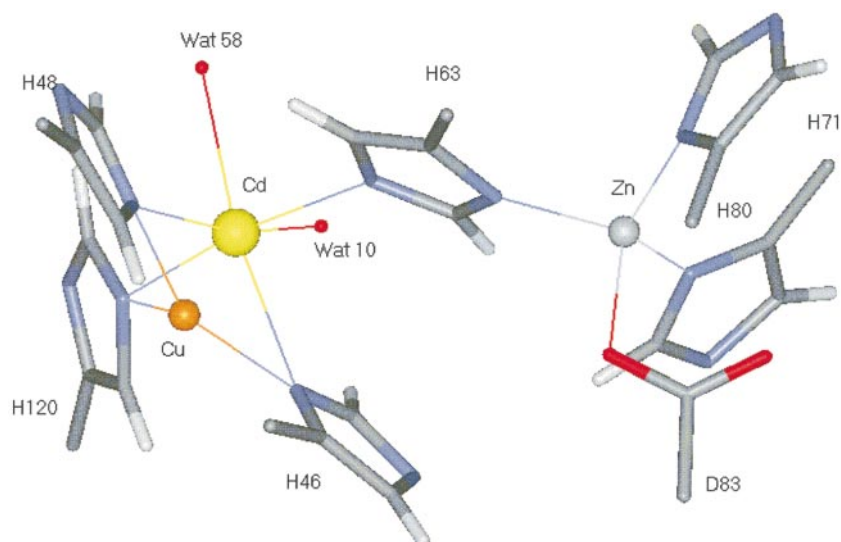


Figure 5. Final model of the active site showing the metal coordination. Larger spheres of arbitrary radius represent copper (orange), cadmium (yellow), and zinc (gray). The cadmium bound water molecules are shown as small red spheres.

by only 0.5 and 0.3 Å, respectively, while His120 is almost unchanged. Interestingly, the copper site is almost superimposable to that found in the natural monomeric Cu,ZnSOD from *E. coli* (Pesce *et al.*, 1997). The two metal ions are 6.72 Å apart, compared to 6.1 Å in the human oxidized dimeric WT SOD (Parge *et al.*, 1992). The differences in the histidine positions result in an overall enlargement of the metal cavity diameter by about 0.50 Å with respect to the WT which may be responsible for a looser copper binding and its partial replacement by cadmium. Weak binding of copper is also suggested by the bond distances between 1.99 and 2.20 Å (Table 1) with an average of 2.08 Å.

Table 1. Bond distances and angles

	Q133M2SOD	ESOD	WT HSOD ^a
A. Bond distances in the coordination sphere of Cu(I) and Zn(II) in the Q133M2SOD mutant determined at 1.02 Å resolution, compared to ESOD and to one subunit of human dimeric oxidized WT SOD (WT HSOD)			
Bond distances (Å)			
Cu-N ⁰¹ His46	1.99	2.19	2.07
Cu-N ⁰² His48	2.05	2.09	2.06
Cu-N ⁰² His120	2.20	2.14	2.07
Cu-N ⁰² His63	3.31	2.65	2.21
Zn-N ⁰¹ His63	2.00	2.13	2.10
Zn-N ⁰¹ His71	2.03	1.98	2.06
Zn-N ⁰¹ His80	2.01	1.93	2.04
Zn-O ⁰¹ Asp83	1.97	2.07	1.92
B. Bond distances and angles in the coordination sphere of Cd(II) in the Q133M2SOD mutant determined at 1.02 Å resolution			
Bond distances (Å)			
Cd-N ⁰¹ His46	2.49		
Cd-N ⁰² His48	2.39		
Cd-N ⁰² His120	2.27		
Cd-N ⁰² His63	2.27		
Cd-O-Wat1	2.39		
Cd-O-Wat2	2.59		
^a Taken from Parge <i>et al.</i> (1992).			

The observed distances are longer than expected for a tri-coordinated copper ion in its +1 oxidation state. For comparison, a recent accurate EXAFS determination on a lyophilized, reduced bovine Cu(I),ZnSOD sample has provided an average Cu-N distance of 1.97 Å (Murphy *et al.*, 1997), while in frozen solution the same distance was 1.94 Å (Blackburn *et al.*, 1984).

The active-site-residue positions and the trigonal copper site arrangements are very similar to those observed in the rhombohedral (R32) crystal form of yeast Cu,ZnSOD and to the recently reported structure of the mutant of human Cu,ZnSOD (Ogihara *et al.*, 1996; Hart *et al.*, 1998), found in FALS patients. In these structures the shortest Cu-N bond distances, in the subunit where copper is found trigonal, range between 2.06 and 2.11 Å and are considered to be consistent with copper(I). The same arrangement of the active-site ligands and of Cu and Zn atoms, is observed in the solution structure of the reduced mutant monomer determined by NMR, where the Cu atom is tri-coordinate (Banci *et al.*, 1998) as well as in the crystal structure of the natural monomeric periplasmic Cu,Zn SOD from *E. coli* (Pesce *et al.*, 1997). In order to shed light on this seemingly erratic behavior of the copper coordination found in these crystal structure determinations, we monitored the copper edge of a polycrystalline sample of Q133M2SOD using XAS spectroscopy. The crystals were from a batch obtained from the same crystallization conditions used for the present structural determination. On irradiation with synchrotron light, a fraction of the copper undergoes photoreduction as evidenced by the copper K-edge of the exposed crystals reported in Figure 6. After 40' of irradiation by the X-ray beam from the bending magnet of the DORIS III synchrotron, a peak at about 8983 eV, assigned to a 1s → 4p transition characteristic of Cu(I) (Kau *et al.*, 1987; Murphy *et al.*, 1997), start to appear in the copper edge accompanied by a decrease of the

white line intensity. The $1s \rightarrow 4p$ peak intensity increases in the first eight hours of exposure and then varies little during the next ten hours (see Figure 6). The intensity of this transition is proportional to the concentration of the Cu(I) species in the sample which can be estimated to reach between 20-30% of the total copper after 18 hours of exposure. This finding is analogous to what has been observed both on a frozen solution and on crystals of a prokaryotic Cu,ZnSOD exposed to synchrotron radiation (Stroppolo *et al.*, 1998) and may provide a possible explanation for the observed phenomena relative to the His63 detachment from copper.

The active site channel

The active site channel is formed by part of loop IV (residues 52-60) and of loop VII (residues 130-143). The latter loop contains several charged, well-conserved residues which provide the electrostatic potential to drive the substrate to the reaction site (Sines *et al.*, 1990). This loop is well ordered and the residues Thr137, Glu132, Lys136, and Gln133 show well-defined electron density in the $3F_o - 2F_c$ map and side-chain

conformations similar to those found in the human native enzyme.

In contrast, the side-chain of Arg143, the residue responsible for the correct orientation of superoxide in the catalytic cavity and which is completely conserved, is highly disordered. The electron density for the side-chain, starting from the C^γ atom on, is very poor in the $3F_o - 2F_c$ map (the average B value for the side-chain atoms is 66.8 \AA^2). The disorder of Arg143 may be related to the absence of the structurally relevant hydrogen bond linking its N^ϵ atom to the carbonyl oxygen atom of Cys57 in the WT in one of the modeled conformations of loop IV.

Loop IV, where two of the mutations lie, is the most disordered part of the structure. Overall, the loop appears loosened with respect to the WT with largely different conformations of residues 48-62, not only in the side-chains, but also in the backbone. The structural relevant H-bond between the carbonyl of Cys57 and N^ϵ of Arg143, which stabilizes the conformation of the latter residue in the electrostatic loop, is present for only one of the conformations of Cys57. Differences compared to WT SOD are also observed in loop VII for residues 129-131.

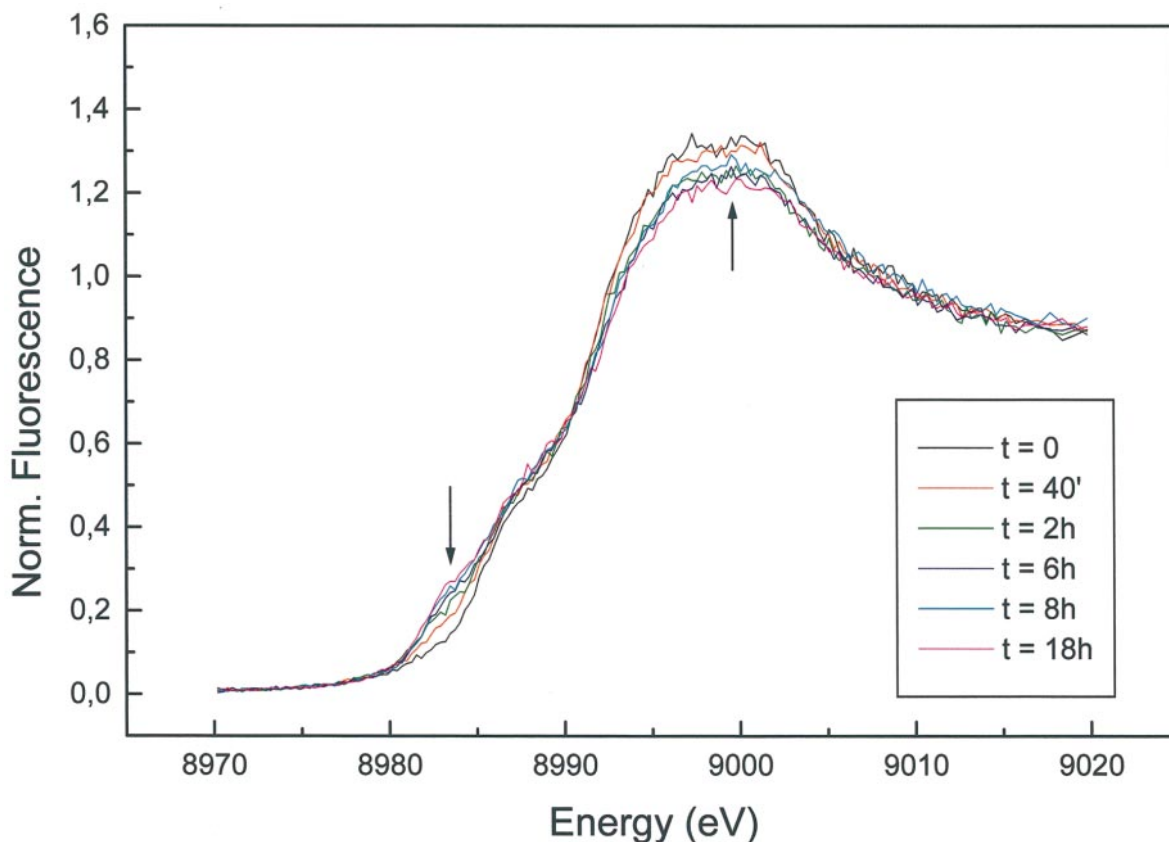


Figure 6. X-ray fluorescence of Q133M2SOD polycrystalline sample at the copper edge recorded at different exposure times. The sample has been exposed to the synchrotron beam for 18 hours. The spectra are colour coded on the basis of the exposure times as shown in the inset. Arrows mark the $1s \rightarrow 4p$ transition at 8983 eV and the absorption maximum at 8998 eV.

As a result of loop IV movement, the width and the depth of the active site cavity are slightly increased with respect to the WT. The cavity is now about 23 Å wide and 13 Å deep compared with 21 Å and 11 Å in the WT (Parge *et al.*, 1992). In addition the distance between the C α atoms of Thr137 and Arg143, which define the second active site pit, has increased by about 2 Å with respect to the WT (Parge *et al.*, 1992). Interestingly, these results sharply contrast with the reduced monomer solution structure where an opposite behavior is observed. Indeed, in that structure, the width of the shallow crevice is decreased by about 3 Å with respect to the human oxidized dimeric enzyme (Banci *et al.*, 1998). As in other crystal structure determinations of Cu,ZnSOD (Rypniewski *et al.*, 1995; Djinovic *et al.*, 1996), the active site channel presents the characteristic chain of well-ordered water molecules linking the metal sites to the surface of the protein.

Discussion

Comparison of the active site channel between monomeric and dimeric forms

The crystallographic study on the Q133M2SOD mutant provides an accurate model for this protein, in addition to its solution structure which has been recently solved (Banci *et al.*, 1998). This is the first X-ray structure at atomic resolution of a SOD enzyme.

The monomeric Cu,ZnSOD from the periplasmic space of an *E. coli* strain has a catalytic activity comparable to that of the other dimeric isoenzymes (Battistoni & Rotilio, 1995). In contrast, the present mutant has a reduced catalytic activity, around 20% that of the WT, even if the substitution E133Q enhances activity two- to threefold with respect to the double mutant F50E/G51E (Banci *et al.*, 1995).

It is well known that Cu,ZnSOD enzymatic activity is highly influenced by the electrostatic field present in the active-site channel that guides the diffusion of the substrate in the active site towards the copper ion (Bertini *et al.*, 1998). Two parts of the molecule in each subunit are involved in the formation of this channel: (1) loop VII in which negatively and positively charged residues form the correct electrostatic field to attract the anionic substrate, and (2) the region of the disulfide bond (Cys57-Cys146) in the loop IV (residues 50-70). In the present structure, the latter region is the one that exerts the most relevant conformational changes with respect to the dimeric enzyme and it is very disordered. Analogous disorder and structural changes with respect to the dimeric form have been found in the solution structure of the same protein segment 50-69 (Banci *et al.*, 1998).

The conformational changes in this region of the loop IV could be relevant in explaining the differences in activity of Q133M2SOD with respect to the native enzyme. Indeed, in the wild-type enzyme, Arg143 interacts with loop IV by forming

a hydrogen bond with the carbonyl oxygen atom of Cys57. This H-bond is important in fixing the position of Arg143 in the cavity. The disorder of the side-chain of this catalytically important residue originates from the high flexibility of the disulfide region in the loop IV. A relatively large disorder for the side-chain of Arg143 was observed in the solution structure (Banci *et al.*, 1998). The conformation that we modeled for the residues around Cys57 (residues 53-61) is only one among the multiple conformations for this region of the crystal structure. Moreover, one of the two conformations found for the side-chain of Cys146 presents the disulfide bond broken. In contrast, in solution the disulfide bridge appears to be always fully formed (Banci *et al.*, 1998).

In the presence of the substantial disorder of Cys57, the Arg143 side-chain may no longer be tied to the loop IV and this could be the reason for its high degree of mobility. The conformation that we modeled for the disulfide region of the loop IV and for the Arg143 side-chain is different from that found in the WT and is not optimal for binding the substrate and correctly orienting it in the enzymatic cavity. This can therefore explain the reduced enzymatic activity of the engineered monomeric forms of Cu,ZnSOD.

This interpretation is further supported by the comparison with the X-ray structure of the natural monomeric *E. coli* Cu,ZnSOD (Pesce *et al.*, 1997). In the latter protein loop IV is disordered, like in Q133M2SOD. However, the Arg143 side-chain in ESOD is ordered and has the same conformation as in the WT eukaryotic enzymes due to a salt link with the nearby Glu residue which lies outside of the disordered loop region (Pesce *et al.*, 1997). Therefore, despite the relatively low degree of homology in loop IV between the two protein families, the key residues in the active-site channel experience a very similar conformation, thus supporting very similar catalytic properties.

The slightly altered structure of the copper binding site could affect the affinity of copper for its binding site as shown by its replacement by 300 mM cadmium(II). The atomic resolution structure has revealed a slightly enlarged cavity at the metal site and the change can be correlated with the different conformations of loop IV. Even small differences in the site structure appear to be crucial in determining the binding of the essential copper. Furthermore, the disorder in the cavity involves only the metal atoms, while all the ligands appear to be well ordered. Consequently, it appears that the site conformation is such as to cause a more open and broader coordination site for copper and hence to favor tri-coordination.

The catalytic mechanism beyond the various structural data

All the X-ray reports on the native enzyme and the NMR data on Cu₂Co₂SOD in solution demonstrate that, as long as copper is oxidized, it is

coordinated to four His residues and that it is connected to zinc through a bridging His residue (Bertini *et al.*, 1998). When Cu(II) is allowed to react with O_2^- , an electron flows from O_2^- to Cu(II), thus providing Cu(I) and O_2 , the latter as a product of the enzymatic reaction. Cu(I) is reported in model complexes to be either trigonal planar or tetrahedral (Orpen *et al.*, 1989), that indicates that the two stereochemistries have similar energies. In Cu,ZnSOD the trigonal planar arrangement is obtained through a migration of the copper ion of about 1 Å which is accompanied by protonation of the histidinato ligand. The resulting structure is shown in Figure 5 where the cadmium, mimicking the Cu(II) site, is bound to four His residues, whereas the copper, presumably reduced, is trigonal planar and His63 moves slightly away to permit its protonation. The energy barrier accompanying the electron transfer process is low because Cu(I) chooses one of its preferred coordinations by binding to three histidine residues and by loosening the Cu-His63 bond. Rotation of His63 and its protonation have minor energetic barriers.

The rate limiting step in the oxidation of O_2^- is its diffusion inside the active cavity, which is higher than its diffusion in bulk water. O_2^- approaches Cu^{2+} until a distance is reached which allows electron transfer without the need of formation of a chemical bond, as implied in other mechanisms (Tainer *et al.*, 1983; Osman & Basch, 1984). It is important that no water molecule is coordinated to copper which should then be easily removed by O_2^- , and that the geometry of the ligands is favorable for the approach. The catalytic center in the reduced form has essentially the same electrostatic field as the oxidized form, as the total charge is the same, and attracts O_2^- with the same rate as the oxidized form. Indeed, kinetic data on samples initially containing only oxidized or only reduced forms of the enzyme and low concentration of O_2^- , have shown that oxidized and reduced forms have the same reaction rates (Rotilio *et al.*, 1972; Klug *et al.*, 1972; Klug-Roth *et al.*, 1973). When the O_2^- anion approaches the reduced form, it encounters on its way the proton bound to the His63 $N^{\epsilon 2}$ atom which lies on top of the Cu(I) ion. The electron transfer rate from Cu(I) to O_2^- can be enhanced by the electrostatic interaction of O_2^- with the protonated His63. Once Cu(II) is formed, it tends to bind His63 whose proton would be transferred to the just formed O_2^{2-} . The shuttle of a proton from $N^{\epsilon 2}$ of His63 to O_2^- would be the barrier for the reforming of the Cu(II)- $N^{\epsilon 2}$ (His63) bond. As already mentioned, the rate-limiting step under low concentrations of O_2^- is its diffusion. At high concentrations of O_2^- the rate-limiting step becomes the proton transfer, as evidenced by the H/D isotope effect on the catalytic rates (Fee & Bull, 1986). All the steps of the complete reaction have such a small energy barrier that the proton diffusion rate becomes the limiting process, as in other diffusion controlled reactions (Fersht, 1985). When O_2^- approaches Cu(I) and encounters the protonated

His63, as shown by the present and the solution structure (Banci *et al.*, 1998), its distance is such that the electron transfer process can occur. The formation of Cu(II) and HO_2^- may be followed by a proton release from the chain of water molecules, repeatedly observed in the X-ray structures of dimeric Cu,ZnSODs (Rypniewski *et al.*, 1995; Djinojic *et al.*, 1996) as well as in the present structure, and H_2O_2 is released, being not bonded to Cu(II) anymore, just like a water molecule.

Conclusions

Here, we report the X-ray structure of a monomeric form of Cu,ZnSOD which contains both a cadmium site and a copper site. The former mimics the oxidized form and the latter the reduced one, thus allowing us to make a meaningful comparison of the two oxidation states. In other dimeric forms of the enzyme, tetra and a tri-coordinated species are contemporarily present in the different subunits of the same dimer (Ogihara *et al.*, 1996; Hart *et al.*, 1998; Ferraroni *et al.*, 1998). The starting crystallization solutions contained the reduced form in one case and the oxidized form in the others. It appears that the occurrence of the tri-coordinate Cu(I) or tetra-coordinate Cu(II) structure can be influenced by crystal forces and molecular mobility. In one case reduction is proposed to occur during the crystallization process (Ogihara *et al.*, 1996). In other cases copper(I) is proposed to have the same stereochemistry of copper (II) (Rypniewski *et al.*, 1995; Ferraroni *et al.*, 1998). In this respect, the solution data are quite informative as packing forces are absent. In solution, every time a reduced species is analyzed, copper is found to be tri-coordinate and every time an oxidized species is determined, copper is found coordinated to the four His residues (Bertini *et al.*, 1998). The X-ray data, on the other hand, suffer from the high X-ray irradiation which can produce photoreduction of the sample which, however, has never been seen as complete.

Indeed, in some of the recently reported crystal structures the Cu-His63 $N^{\epsilon 2}$ bond is lengthened or broken. However, this occurred, with the exception of the R32 crystal form, in Cu,ZnSODs which are either monomeric or characterized by crystal packings involving subunit-subunit interactions different from that observed in WT HSOD and/or high mobility. The two monomeric forms so far determined share the disorder of loop IV, while the dimeric ones are characterized by high mobility. These structural aspects may make accessible coordination geometries which may favor photoreduction of copper(II).

The present structural report on a monomeric form is relevant for several reasons. First of all, it definitely demonstrates that a monomeric form has been obtained. Secondly, the presence of copper and cadmium ions at the active site is mimicking the reduced and the oxidized metal coordination

geometry at the same time. The comparison with the many available X-ray structures has allowed us to rationalize the structural properties of SOD, beyond the individual structures and to propose a more detailed enzymatic mechanism. Thirdly, both X-ray and solution data show that the mutations needed to produce a monomeric species induce disorder at the potential subunit interface which can be interpreted as being due to local mobility. It is well known that enzymes need to take the optimal conformation to accomplish the biological function. Loops are much more flexible than other parts of the protein and their conformation is the result of fine balance of many structural features. The disorder, on its turn, induces disorder on the catalytically relevant charged groups in the active site channel. The disorder observed in this structure is completely consistent with what observed in the solution structure (Banci *et al.*, 1998).

This aspect raises the question why eukaryotic SOD is essentially found as a multimeric enzyme. It is possible that dimeric species are needed because subunit-subunit interactions can determine the correct geometry of the cavity and the optimal orientation of the charged residues in the active channel. In particular Arg143, which plays a strategic role in the enzyme mechanisms (Bertini *et al.*, 1998), has a precise position in the dimeric protein while it is disordered in the present monomer, both in the crystal and in the solution. The disorder of Arg143 is probably due to the absence of an H-bond between its N^ε with the carbonyl group of Cys57 which, in the present monomeric form, exhibit conformational disorder. The low number of nuclear Overhauser enhances observed in the solution structure determination of the same monomer for the residues 50-60 has been interpreted as due to local mobility (Banci *et al.*, 1998). The disorder and the subsequent change in the electrostatic field can well account for the low activity of the present monomeric form. The relevance of the structure determination of SOD monomeric forms is also related to the occurrence of this species in the periplasmic space of an *E. coli* strain and to the fact that mutations similar to those which give rise to monomers are found in FALS disease. In the natural monomeric form, which has catalytic efficiency identical with the dimeric Cu,ZnSOD, sequence changes have been developed in the protein such as to maintain the correct conformation of the relevant residues in catalysis. On the contrary, the monomeric species isolated in FALS disease patients and which has a reduced activity, could present disorder and structural changes similar to those observed in the present monomeric form.

Materials and Methods

Protein preparation and crystallization

The monomeric mutant Q133M2SOD was prepared and purified as reported (Banci *et al.*, 1995). An enzy-

matic activity of 20% that of the WT enzyme was measured at pH 7.5 by described procedures (Banci *et al.*, 1995). The protein concentration was calculated from the UV-spectrum using a molar absorption coefficient of 7400 cm⁻¹ at 265 nm. Diffraction quality crystals of the mutant were obtained by the hanging drop method. A 5 μl sample of a 15 mg/ml protein solution in 20 mM Tris-HCl (pH 7.5) was mixed with an equal volume of 15% (v/v) PEG 6000, 200-400 mM CdCl₂ in 100 mM Tris-HCl (pH 8.0) and equilibrated against 1 ml of the latter solution. Regularly shaped prismatic light blue crystals appeared after a few days at 4 °C. The effectiveness of cadmium ions in promoting crystallization due to their ability to bind carboxylate groups of residue side-chains on the protein surface, has been recently demonstrated (Trakhanov & Quioco, 1995). The crystals belong to the orthorhombic space group *P*2₁2₁2₁ with cell dimensions *a* = 34.54 Å, *b* = 47.73 Å, *c* = 81.36 Å. Assuming a molecular mass of about 16 kDa and one molecule in the asymmetric unit, the packing density, *V*_{mv} is 2.13 Å³/Da corresponding to a solvent content of 42% (Matthews, 1968).

Data Collection

A first complete data set extending to 1.4 Å resolution was collected at 100 K using radiation ($\lambda = 1.0$ Å) from the synchrotron ELETTRA in Trieste and a 18 cm MarResearch image plate scanner. The crystal was treated with a cryoprotectant solution obtained by adding 20% (v/v) ethylene glycol to the harvest solution. Data were collected with the rotation technique, from a single crystal in two passes, with shorter exposure time at low resolution to ensure measurement of strong reflections overloaded in the high resolution data set. The DENZO (Otwinowski, 1993) package was used for intensity integration and scaling. A summary of the data collection and processing is given in Table 2A.

A second complete data set at atomic resolution (1.02 Å) was collected using cryocooling techniques and synchrotron radiation from the EMBL beamline BW7B at the DORIS storage ring, DESY, Hamburg. Data were collected using a 30 cm MarResearch imaging-plate in three passes, and the wavelength used was 0.89 Å. Data processing with the same program as before gave 69,897 unique reflections with an *R*_{symm} of 0.061 and an overall completeness of 99.1%. A summary of the data collection and processing is given in Table 2B.

Structure solution and refinement

The 1.4 Å data set was used for the structure solution by molecular replacement with the program AMoRe (Navaza, 1994) from the CCP4 (Collaborative Computational Project, 1994) program suite applied to the 10.0-3.5 Å resolution data with a Patterson radius of 18 Å. A model for the monomeric enzyme was constructed from the atomic coordinates of a single subunit of the native human SOD (1SOS) deposited in the Brookhaven Protein Data Bank (Bernstein *et al.*, 1977). The peak corresponding to the correct orientation in the rotation function map was at the 6.5 σ level, 1.5 times higher than the next peak. The translation search gave a solution with *R* = 0.43, a correlation coefficient of 0.45 and a reasonable molecular packing. Rigid body refinement lowered the *R*-factor to 0.41. Inspection of the 3*F*_o - 2*F*_c Fourier map showed good agreement of the enzyme β -barrel

Table 2. Summary of the data collection and processing

A. ELETTRA			
	High-resolution data set	Low-resolution data set	
Wavelength (Å)	1.0	1.0	
Maximum resolution	1.4	4.1	
Oscillation per image (°)	1.0	3.0	
Number of images	105	35	
Number of raw measurements	149,862		
Number of unique reflections collected	25,098		
Resolution range (Å)	10.0-1.43		
Completeness for range (%)	98.1		
R_{symm}	0.066		
Average $I/\sigma(I)$ for the data set	14.7		
Data quality in the high-resolution shell			
Resolution range (Å)	1.6-1.4		
Completeness (%)	95.0		
R_{symm}	0.263		
$I/\sigma(I)$	3.1		
B. DESY			
	High-resolution data set	Medium-resolution data set	Low-resolution data set
Wavelength (Å)	0.889	0.889	0.889
Maximum resolution	1.0	1.45	2.95
Oscillation per image (°)	0.5	1.0	2.0
Number of images	128	91	46
Exposure time	240	30	15 ^a
Number of raw measurements	681,833		
Number of unique reflections collected	69,841		
Resolution range (Å)	20.0-1.02		
Completeness for range (%)	99.1		
R_{symm}	0.061		
Average $I/\sigma(I)$ for the data set	37.9		
Data quality in the high-resolution shell			
Resolution range (Å)	1.04-1.02		
Completeness (%)	98.0		
R_{symm}	0.247		
$I/\sigma(I)$	2.2		

^aAluminium foils to attenuate intensity.

model with electron density, but poor density for most of the loop regions.

Crystallographic refinement was carried out with the CCP4 version of PROLSQ (Konnert, 1976; Konnert & Hendrickson, 1980) against 95% of the data. The remaining 5% (approximately 1500 reflections) randomly excluded from the data set were used to follow the progress of the refinement with R_{free} . The R -factor converged to 0.218 after several rounds of stereochemically restrained least-squares refinement followed by manual rebuilding based on $3F_o - 2F_c$ and $F_o - F_c$ maps, using the programs FRODO and O (Jones, 1978; Jones *et al.*, 1991). Solvent molecules were inserted using the program ARP (Lamzin & Wilson, 1993) and refined with occupancy set to 1.0. SHELXL96 (Sheldrick & Schneider, 1997) was then used to refine the structure with anisotropic temperature factors for metal ions. Besides the active site Cu(II), Cd(II) and Zn(II) ions, eight Cd(II) ions bound to negative charged residues

Table 3. Refinement and atomic resolution statistics

A. Refinement statistics			
Resolution limits (Å)			10.0-1.43
Protein atoms			1067
Water molecules			183
Metal ions			11
R (%)			20.1
R_{free} (%)			22.7
Stereochemistry		weight	rms
Bond length (1-2 neighbors) (Å)	0.020		0.028
Angle distance (1-3 neighbors) (Å)	0.040		0.059
Dihedral angles (1-4 neighbors) (Å)	0.050		0.066
Chiral volumes (Å ³)	0.12		0.16
Planar torsion angles (deg.)	10.0		4.4
Deviation from planes (Å)	0.020		0.022
B. Atomic resolution refinement statistics			
Resolution limits			20.0-1.02
Protein atoms			1166
Solvent molecules			284
Metal ions and others			13
R (%)			11.8
Data/parameters ratio (aniso)			5.5

on the enzyme's surface were found. The R -factor converged to 0.201 and R_{free} was 0.227. The statistics for refinements are reported in Table 3A and B, respectively.

Atomic resolution refinement

Refinement at atomic resolution was performed starting from the final model of the above refinement and used SHELXL96. Anisotropic temperature factors were refined for each atom of the protein and solvent molecules using default restraints. Occupancy factors for disordered parts of the model and for metal ions were refined. Alternative conformations were modeled for 13 side-chains constraining the sum of the two components to one. Solvent molecules were introduced using the program ARP. The refinement of the enzyme molecule, 284 water molecules and 11 metal ions, against data in the 20.0-1.02 Å resolution range, converged to an R -factor of 0.118. Standard deviations for the coordinates and anisotropic temperature factors were estimated from a block-matrix unrestrained least-squares cycle where each block consisted of 20 residues overlapping by one residue with the adjacent blocks.

X-ray absorption spectroscopy

A polycrystalline sample of Q133M2SOD crystals, grown in the same conditions as the crystals used for X-ray crystallography, has been used to monitor the X-ray fluorescence at the copper edge. XAS measurements were performed at the EMBL EXAFS beamline (c/o DESY, Hamburg). During the experiments the DORIS III storage ring was operating in dedicated mode at 4.5 GeV with ring currents ranging from 80 to 140 mA. A Si(111) double crystal monochromator with an energy resolution of 1.6 eV at 8980 eV was used. The second monochromator crystal was detuned to 50% of its peak intensity in order to reject higher harmonics. The monochromator angle was converted to an absolute

energy scale by using a calibration technique (Pettifer & Hermes, 1985). The sample fluorescence was detected with an energy discriminating 13 element Ge solid-state detector. The data were collected at the copper edge (8986.0 eV at the edge jump inflection point). The spectrum was recorded from 8930 to 9810 eV with variable step widths. In the XANES and EXAFS regions steps of 0.3 and 0.6-1.5 eV were used respectively. A series of 21 spectra were collected on the frozen crystals at 20 K for a maximum exposure to X-rays of 18 hours. After inspection of each scan for edge consistency, the data were normalized by considering the atomic background before and after the edge.

Protein Data Bank accession number

The atomic coordinates and structure factors of the Q133M2SOD structure have been deposited with the Brookhaven Protein Data Bank (Bernstein *et al.*, 1977) under the accession code 1mfm.

Acknowledgments

We thank Dr Wolfram Meyer-Klaucke from the Hamburg EMBL Outstation for the help in collecting the XAS data. The authors thank the European Union for support of the work at EMBL Hamburg through the HCMP Access to Large Installation Project, Contract Number CHGE-CT93-0040. Financial support from Italian CNR, Comitato Scienze Chimiche and Progetto Strategico "Tecnologie Chimiche Innovative", and from Italian MURST (ex 40%) is also acknowledged.

References

- Banci, L., Bertini, I., Hallewell, R. A., Luchinat, C. & Viezzoli, M. S. (1989a). Water in the active cavity of copper/zinc superoxide dismutase. A water ^1H -nuclear-magnetic-relaxation-dispersion study. *Eur. J. Biochem.* **184**, 125-129.
- Banci, L., Bertini, I., Luchinat, C., Piccioli, M., Scozzafava, A. & Turano, P. (1989b). ^1H NOE studies on dicopper(II) dicobalt(II) superoxide dismutase. *Inorg. Chem.* **28**, 4650-4656.
- Banci, L., Carloni, P., La Penna, G. & Orioli, P. L. (1992). Molecular dynamics studies on superoxide dismutase and its mutants: the structural and functional role of Arg 143. *J. Am. Chem. Soc.* **114**, 6994-7001.
- Banci, L., Bertini, I., Luchinat, C., Piccioli, M. & Scozzafava, A. (1993). 1D versus 2D ^1H NMR experiments in dicopper, dicobalt superoxide dismutase: a further mapping of the active site. Dedicated to Professor Lamberto Malatesta. *Gazz. Chim. Ital.* **123**, 95-100.
- Banci, L., Carloni, P. & Orioli, P. L. (1994). Molecular dynamics studies on mutants of Cu,Zn Superoxide Dismutase: the functional role of charged residues in the electrostatic loop VII. *Proteins: Struct. Funct. Genet.* **18**, 216-230.
- Banci, L., Bertini, I., Chiu, C. Y., Mullenbach, G. T. & Viezzoli, M. S. (1995). Synthesis and characterization of a monomeric mutein of Cu/Zn superoxide dismutase with partially reconstituted enzymatic activity. *Eur. J. Biochem.* **234**, 855-860.
- Banci, L., Bertini, I., Viezzoli, M. S., Argese, E., Orsega, E., Chui, Y. C. & Mullenbach, G. T. (1997). Tuning the activity of Cu,Zn superoxide dismutase through site directed mutagenesis: a relatively active monomeric species. *J. Inorg. Biochem.*, **2**, 295-301.
- Banci, L., Benedetto, M., Bertini, I., Del Conte R., Piccioli, M. & Viezzoli, M. S. (1998). The solution structure of reduced monomeric Q133M2 superoxide dismutase. Why is SOD a dimeric enzyme? *Biochemistry*, **37**, 11780-11791.
- Bannister, J. V., Bannister, W. H. & Rotilio, G. (1987). Aspects of the structure, function and applications of superoxide dismutase. *CRC Crit. Rev. Biochem.* **22**, 111-180.
- Battistoni, A. & Rotilio, G. (1995). Isolation of an active and heat-stable monomeric form of Cu,Zn superoxide dismutase from the periplasmic space of *Escherichia coli*. *FEBS Letters*, **374**, 199-202.
- Bernstein, F. C., Koetzle, T. F., Williams, G. J. B., Meyer, E. F., Jr, Rodgers, , Kennard, O., Shimanouchi, T. & Tasumi, M. (1977). The Protein Data Bank: a computer-based archival file for macromolecular structure. *J. Mol. Biol.* **112**, 535-542.
- Bertini, I., Luchinat, C. & Monnanni, R. (1985). Evidence of the breaking of the copper-imidazolate bridge in copper/cobalt-substituted superoxide dismutase upon reduction of the copper(II) centers. *J. Am. Chem. Soc.* **107**, 2178-2179.
- Bertini, I., Luchinat, C., Piccioli, M., Vicens, Oliver M. & Viezzoli, M. S. (1991). ^1H NMR investigation of reduced copper-cobalt superoxide dismutase. *Eur. Biophys. J.* **20**, 269-279.
- Bertini, I., Piccioli, M., Scozzafava, A. & Viezzoli, M. S. (1993). Copper, cobalt, superoxide dismutase: a reexamination of the ^1H NMR spectrum through a novel selectively deuterated derivative. *Magn. Reson. Chem.* **31**, S17-S22.
- Bertini, I., Piccioli, M., Viezzoli, M. S., Chiu, C. Y. & Mullenbach, G. T. (1994). A spectroscopic characterization of a monomeric analog of copper-zinc superoxide dismutase. *Eur. J. Biophys.* **23**, 167-176.
- Bertini, I., Mangani, S. & Viezzoli, M. S. (1998). Structure and properties of copper-zinc superoxide dismutases. In *Advances in Inorganic Chemistry* (Sykes, L., ed.), pp. 127-250, Academic Press, New York.
- Blackburn, N. J., Hasnain, S. S., Binsted, N., Diakun, G. P., Garner, C. D. & Knowles, P. F. (1984). An extended-X-ray-absorption-fine-structure study of bovine erythrocyte superoxide dismutase in aqueous solution. *Biochem. J.* **219**, 985-990.
- Bourne, Y., Redford, S. M., Steinmann, H. M., Lepock, J. R., Tainer, J. A. & Getzoff, E. D. (1996). Novel dimeric interface and electrostatic recognition in bacterial Cu,Zn superoxide dismutase. *Proc. Natl Acad. Sci. USA*, **93**, 12774-12779.
- Chen, Y.-L., Park, S., Thornburg, R. W., Tabatabai, L. B. & Kintanar, A. (1995). Structural characterization of the active site of *Brucella abortus* Cu-Zn superoxide dismutase: A ^{15}N and ^1H NMR investigation. *Biochemistry*, **34**, 12265-12275.
- Collaborative Computational Project No. 4 (1994). The CCP4 suite: programs for protein crystallography. *Acta Crystallog. sect. D*, **50**, 760-763.
- Djinovic, C., Battistoni, A., Carri, M., Polticelli, F., Desideri, A., Rotilio, G., Coda, A., Wilson, K. & Bolognesi, M. (1996). Three-dimensional structure of *Xenopus laevis* Cu,ZnSOD b determined by X-ray

- crystallography at 1.5 Å resolution. *Acta Crystallog. sect. D*, **52**, 176-188.
- Djinovic, K., Gatti, G., Coda, A., Antolini, L., Pelosi, G., Desideri, A., Falconi, M., Marmocchi, F., Rotilio, G. & Bolognesi, M. (1992). Crystal structure of yeast Cu,Zn superoxide dismutase. Crystallographic refinement at 2.5 Å resolution. *J. Mol. Biol.* **225**, 791-809.
- Fee, J. A. & Bull, C. (1986). Steady-state kinetic studies of superoxide dismutases. *J. Biol. Chem.* **261**, 13000-13005.
- Ferraroni, M., Rypniewski, W., Bruni, B., Orioli, P. & Mangani, S. (1998). Crystallographic determination of reduced bovine superoxide dismutase at pH 5.0 and of anion binding to its active site. *J. Inorg. Biochem.*, **3**, 411-422.
- Fersht, A. R. (1985). *Enzymes, Structure and Mechanism*, Freeman, New York.
- Fridovich, I. (1995). Superoxide radical and superoxide dismutases. *Annu. Rev. Biochem.* **64**, 97-112.
- Getzoff, E. D., Tainer, J. A., Stempien, M. M., Bell, G. I. & Hallewell, R. A. (1989). Evolution of CuZn superoxide dismutase and the greek key β -barrel structural motif. *Proteins: Struct. Funct. Genet.* **5**, 322-336.
- Hart, P. J., Liu, H., Pellegrini, M., Nerissian, A. M., Gralla, E. B., Valentine, J. S. & Eisenberg, D. (1998). Subunit asymmetry in the three-dimensional structure of a human CuZnSOD mutant found in a familial amyotrophic lateral sclerosis. *Protein Sci.* **7**, 545-555.
- Jones, T. A. (1978). A graphics model building and refinement system for macromolecules. *J. Appl. Crystallog.* **11**, 268-272.
- Jones, T. A., Cowan, S. W. & Kjeldgaard, M. (1991). Improved methods for building protein models in electron density maps and the location of errors in these models. *Acta Crystallog. sect. A*, **47**, 110-119.
- Kau, L. S., Spira-Solomon, D. J., Penner-Hahn, J. E., Hodgson, K. O. & Solomon, E. I. (1987). X-ray absorption edge determination of the oxidation state and coordination number of copper: application to the type 3 site in *Rhus vernicifera* laccase and its reaction with oxygen. *J. Am. Chem. Soc.* **109**, 6433-6442.
- Klug, D., Rabani, J. & Fridovich, I. (1972). A direct demonstration of the catalytic action of superoxide dismutase through the use of pulse radiolysis. *J. Biol. Chem.* **247**, 4839-4842.
- Klug-Roth, D., Fridovich, I. & Rabani, J. (1973). Pulse radiolytic investigation of superoxide catalyzed disproportionation. mechanism for bovine superoxide dismutase. *J. Am. Chem. Soc.* **95**, 2786-2790.
- Konnert, J. H. (1976). A restrained-parameter structure-factor least-squares refinement procedure for large asymmetric units. *Acta Crystallog. sect. A*, **32**, 614-617.
- Konnert, J. H. & Hendrickson, W. A. (1980). A restrained-parameter thermal-factor refinement procedure. *Acta Crystallog. sect. A*, **36**, 344-350.
- Lamzin, V. S. & Wilson, K. S. (1993). Automated refinement of protein models. *Acta Crystallog. sect. D*, **49**, 129-147.
- Laskowski, R. A., MacArthur, M. W., Moss, D. S. & Thornton, J. M. (1993). PROCHECK: a program to check the stereochemical quality of protein structures. *J. Appl. Crystallog.* **26**, 283-291.
- Matthews, B. W. (1968). Solvent content of protein crystals. *J. Mol. Biol.* **33**, 491-497.
- McAdam, M. E., Fielden, E. M., Lavelle, F., Calabrese, L., Cocco, D. & Rotilio, G. (1977). The involvement of the bridging imidazolate in the catalytic mechanism of action of bovine superoxide dismutase. *Biochem. J.* **167**, 271-274.
- Murphy, L. M., Strange, R. W. & Hasnain, S. S. (1997). A critical assessment of the evidence from XAFS and crystallography for the breakage of the imidazolate bridge during catalysis in CuZn superoxide dismutase. *Structure*, **5**, 371-379.
- Navaza, J. (1994). An automated package for molecular replacement. *Acta Crystallog. sect. A*, **50**, 157-163.
- Ogihara, N. L., Parge, H. E., Hart, J. P., Weiss, M. S., Goto, J. J., Crane, B. R., Tsang, J., Slater, K., Roe, J. A. & Valentine, J. (1996). Unusual trigonal-planer configuration revealed in the atomic structure of yeast copper-zinc superoxide dismutase. *Biochemistry*, **35**, 2316-2321.
- Orpen, G., Brammer, L., Allen, F. H., Kennard, O. & Watson, D. G. (1989). Tables of bond lengths determined by X-ray and neutron diffraction. Part 2. Organometallic compounds and coordination complexes of the d- and f-block metals. *J. Chem. Soc.*, S1-S83.
- Osman, R. & Basch, H. (1984). On the mechanism of superoxide dismutase: a theoretical study. *J. Am. Chem. Soc.* **106**, 5710-5714.
- Otwinowski, Z. (1993). Oscillation data reduction program. In *Proceedings of the CCP4 Study Weekend. Data Collection and Processing. 29-30 January 1993* (Sawyer, L., Isaacs, N. & Bailey, S., eds), pp. 56-62, SERCDaresbury Laboratory, Chester.
- Parge, H. E., Hallewell, R. A. & Tainer, J. (1992). Atomic structures of wild-type and thermostable mutant recombinant human Cu,Zn superoxide dismutase. *Proc. Natl Acad. Sci. USA*, **89**, 6109-6114.
- Pesce, A., Capasso, C., Battistoni, A., Folcarelli, S., Rotilio, G., Desideri, A. & Bolognesi, M. (1997). Unique structural features of the monomeric Cu,Zn superoxide dismutase from *Escherichia coli*, revealed by X-ray crystallography. *J. Mol. Biol.* **274**, 408-420.
- Pettifer, R. F. & Hermes, C. (1985). Absolute energy calibration of X-ray radiation from synchrotron sources. *J. Appl. Crystallog.* **18**, 404-412.
- Ramachandran, G. N. & Sasisekharan, V. (1968). Conformation of polypeptides and proteins. *Advan. Protein Chem.* **23**, 283-437.
- Rotilio, G., Bray, R. C. & Fielden, E. M. (1972). A pulse radiolysis study of superoxide dismutase. *Biochim. Biophys. Acta*, **268**, 605-609.
- Rypniewski, W. R., Mangani, S., Bruni, B., Orioli, P. L., Casati, M. & Wilson, K. S. (1995). Crystal structure of reduced bovine erythrocyte superoxide dismutase at 1.9 Å resolution. *J. Mol. Biol.* **251**, 282-296.
- Sheldrick, G. M. & Schneider, T. R. (1997). SHELXL: high-resolution refinement. *Methods Enzymol.* **277**, 319-343.
- Sines, J. J., Allison, S. A. & McCammon, J. A. (1990). Point charge distribution and electrostatic steering in enzyme/substrate encounter: Brownian dynamics of modified copper/zinc superoxide dismutase. *Biochemistry*, **29**, 9403-9412.
- Stroppolo, M. E., Nuzzo, S., Pesce, A., Rosano, C., Battistoni, A., Bolognesi, M., Mobilio, S. & Desideri, A. (1998). On the coordination and oxidation states of the active-site copper ion in prokaryotic Cu,Zn

- superoxide dismutase. *Biochem. Biophys. Res. Commun.*, **249**, 579-582.
- Tainer, J. A., Getzoff, E. D., Beem, K. M., Richardson, J. S. & Richardson, D. C. (1982). Determination and analysis of 2 Å structure of copper zinc superoxide dismutase. *J. Mol. Biol.* **160**, 181-217.
- Tainer, J. A., Getzoff, E. D., Richardson, J. S. & Richardson, D. C. (1983). Structure and mechanism of copper, zinc superoxide dismutase. *Nature*, **306**, 284-287.
- Trakhanov, S. & Quijcho, S. A. (1995). Influence of divalent cations in protein crystallization. *Protein Sci.* **4**, 1914-1919.

Edited by A. R. Fersht

(Received 20 November 1998; received in revised form 9 March 1999; accepted 9 March 1999)